Gap solitons with quadratic and quartic dispersion competition in one-dimensional nonlinear periodic systems

Y. Cao and T. F. Xu[*]

State Key Laboratory of Metastable Materials Science & Technology and Key Laboratory for Microstructural Material Physics of Hebei Province, School of Science, Yanshan University, Qinhuangdao 066004, People's Republic of China

We studied gap solitons and nonlinear Bloch waves in Kerr nonlinear systems under competition between quadratic and quartic dispersions. The results show that nonlinear Bloch waves can still be regarded as infinite fundamental gap solitons chains. We also revealed the properties of the gap solitons in the relevant band gaps by numerical analysis. Notably, for the two classical dipole modes in the first gap, the variation of the dispersion coefficient leads to the change of the soliton power relation due to the interaction between the two solitons composing them. We obtained the stable interval variation rule of gap waves without calculation by analyzing the interaction between fundamental gap solitons. This is consistent with our linear stability analysis and real-time numerical monitoring results. This finding provides an idea for further investigation of the physical properties of higher-order solitons under higher-order dispersion.

I. INTRODUCTION

As one of the most famous nonlinear phenomena, the soliton has been widely focused on by the scientific community. It is a pulsed traveling wave whose shape, amplitude, and velocity remain unchanged during propagation. Even after two solitons collide, they maintain their respective shapes and velocities. Due to this particular property, it is widely used in fluid mechanics [1], plasma physics [2], Bose-Einstein condensation [3,4], nonlinear optics [5], and other fields [6]. In optics, the optical pulse formed by the nonlinear change of refractive index and the balance of the group dispersion effect is called an optical soliton, usually described by the cubic nonlinear Schrödinger equation. Due to the robust stability of solitons, they are often used as information carriers in information transmission. In the past few decades, researchers have focused on solitons formed by the competition between abnormal quadratic dispersion and the Kerr nonlinear effect [7–10]. The higher-order dispersion is regarded as a disturbance. However, it is well known that higher-order nonlinearity and higher-order dispersion effects are usually not negligible in ultrahigh-bit-rate optical communication systems. The influence of higher-order dispersion on femtosecond (short) pulses applied in ultrafast fiber lasers and other fields cannot be ignored. For example, when the width of short pulses is close to 50 fs, the cubic dispersion plays a vital role in propagation. When the pulse is less than 10 fs, the quartic dispersion effect is also valuable [11,12]. Recently, Ref. [13] showed that pure quartic solitons obtained by quartic dispersion and Kerr nonlinear balance are found in silicon photonic crystal waveguides. Such solitons have the advantage of energy spread over traditional optical solitons with quadratic dispersion and Kerr nonlinearity, allowing higher-energy pulses to be obtained at

short pulse widths. Researchers hope to apply this discovery to fiber lasers [14], but how to manage dispersion in fibers has become an urgent problem, which has led to extensive discussion on higher-order dispersion.

In recent studies, pure cubic solitons [15] and pure quartic solitons [16–18] formed by single dispersion and Kerr nonlinearity have been mentioned constantly. Nevertheless, pure dispersion solitons are challenging to achieve. Many researchers consider combining higher-order dispersion in Kerr media rather than simply treating higher-order dispersion as a disturbance. Surprisingly, in Ref. [19], it was found that compared with pure quadratic or pure quartic dispersion, using the dispersion of different orders is expected to maximize the performance of fiber lasers. Therefore, the scientific community considers various dispersion combinations, such as a quadratic, cubic dispersion combination [20–22], a quadratic, cubic, and quartic dispersion combination [23–27], and even combinations of higher-order dispersions than quartic [28–31]. These studies show that adding higher-order dispersion impacts the solitons' power, shape, and stability. Furthermore, in parity-time ($\mathcal{PT}$) period systems, the addition of quartic dispersion significantly affects the Bloch band structure [32]. The quartic dispersion produces different effects for different $\mathcal{PT}$ potential traps and can even alter the $\mathcal{PT}$-breaking points [33].

In the study of higher-order dispersion, there have been many studies of quadratic and quartic dispersion [34–36]. However, in these works, only the influence of the quartic dispersion coefficient on fundamental gap solitons (FGSs) is considered. This paper details the properties of gap solitons under the Kerr nonlinear effect, quadratic dispersion, and quartic dispersion. In particular, we obtain the stability of gap waves by analyzing the interaction between solitons. In another reference [36], it is also called multipulse solitons. Nonlinear Bloch waves (NBWs) and solitons are the two most typical phenomena in nonlinear periodic systems. We study

_____
[*]tfxu@ysu.edu.cn

the relationship between them and analyze the influence of quadratic and quartic dispersion on the properties of solitons by numerical calculation. The structure of this paper is as follows. In Sec. II, we give the model with quadratic and quartic dispersion under Kerr nonlinearity and define the soliton power. In Sec. III, we use the numerical analysis method to analyze the properties of solitons under higher-order dispersion. For the dipole mode, we regard it as the formation of two FGSs coupling through interaction and analyze the interaction type between solitons. Finally, the relationship between solitons and NBWs is given. In Sec. IV, by analyzing the interaction between two FGSs that make up the dipole mode, we give the stability of the dipole under different parameters and propagation constants, which is consistent with the results obtained by linear stability analysis and real-time evolution. In the following section (Sec. V), we discuss the stability of gap waves constructed by different construction methods in detail. We conclude in Sec. VI.

II. MODEL

In a one-dimensional periodic system, we consider that pulse propagation along the fiber under the combined influence of quadratic dispersion, quartic dispersion, and Kerr nonlinearity is described by the generalized Gross-Pitaevskii equation [19,35,37],

$$i\frac{\partial \psi}{\partial z} = \frac{\beta_2}{2}\frac{\partial^2 \psi}{\partial t^2} - \frac{\beta_4}{24}\frac{\partial^4 \psi}{\partial t^4} + V(t)\psi - \gamma|\psi|^2\psi, \quad (1)$$

with $V(t)$ is a time-periodic function. This paper will use $V(t) = v_0 \sin^2(t)$. $\psi(t, z)$ is the slowly varying complex envelope of the electric field, z is the propagation distance, and t is the retarded time, which is normalized using the optical frequency of the coherent laser. β_2 and β_4 are quadratic and quartic dispersion coefficients, which are indicated by $\partial^2 k/\partial \omega^2$ and $\partial^4 k/\partial \omega^4$, respectively. γ is the normalized Kerr nonlinear coefficient and its sign represents the nonlinear type: $\gamma < 0$ for the defocusing (or repulsive) case and $\gamma > 0$ for the focusing (attractive) case. Here we only consider the defocusing case. For simplicity, we set the Kerr coefficient to -1, namely, $\gamma = -1$. When we select $\gamma = 1$, the soliton can be found in the semi-infinite gap below the first energy band [38], and such solitons are similar to the FGSs of the first energy gap at $\gamma = -1$. In this case, we can consider the semi-infinite gap as the "first energy gap." Usually, such nonlinearity is selected in the study of gap solitons' laws without external potential [39–41] or dark solitons [42].

To obtain the stationary solutions, we use the method of separating variables. Substituting the solution in the form of $\psi(t, z) = \phi(t)\exp(-i\mu z)$ into the generalized nonlinear Schrödinger equation (1) yields a z-independent equation,

$$\mu\phi = \frac{\beta_2}{2}\frac{\partial^2 \phi}{\partial t^2} - \frac{\beta_4}{24}\frac{\partial^4 \phi}{\partial t^4} + v_0 \sin^2(t)\phi - \gamma|\phi|^2\phi. \quad (2)$$

Here, μ is called the propagation constant. Due to the addition of Kerr nonlinear terms, NBWs and FGSs are two essential stationary solutions of Eq. (2). In soliton theory, FGSs can be considered a fundamental component of NBWs. This conclusion is also proper in the case of the quartic dispersion
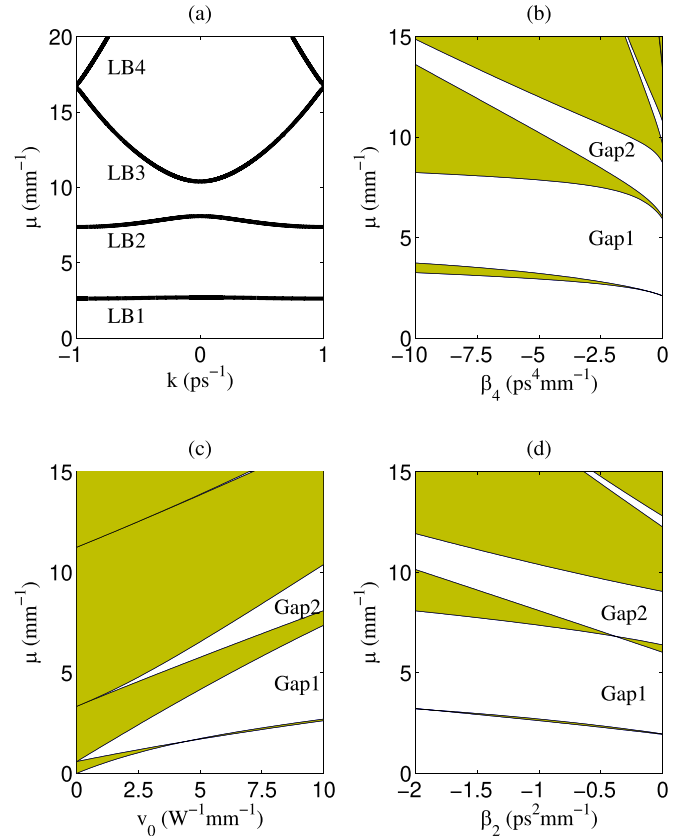

FIG. 1. Bloch energy structure, where LBi represent the ith linear band. (a) $v_0 = 10 \ \text{W}^{-1}\,\text{mm}^{-1}$, $\beta_2 = -1 \ \text{ps}^2\,\text{mm}^{-1}$, and $\beta_4 = -2 \ \text{ps}^4\,\text{mm}^{-1}$. (b)–(d) The shadow areas represent the linear band and the invariant parameters are taken from the parameters in (a).

term, which will be mentioned later. Note that when μ is a purely real number, the intensity of stationary solutions will not change with the propagation of the pulse, namely, $|\psi(t, z)|^2 = |\phi(t)|^2$. In the soliton system, we usually call it the conserved density and can define soliton power as

$$P = \int_{-\infty}^{\infty} |\phi(t)|^2 dt. \quad (3)$$

FGSs will be limited inside a unit cell since the periodic external potential trap exists. In contrast, NBWs are periodically distributed in the entire space. To better find the matching NBWs, we define the average norm of the NBWs by

$$N = \int_{0}^{\pi} |\phi(t)|^2 dt. \quad (4)$$

III. BAND SPECTRUM AND GAP SOLITONS

Since the propagation constant of gap solitons only takes the value within the linear Bloch band gap [43], it is very important to calculate the Bloch energy spectrum. First, we apply Bloch theorem $\phi_{n,k}(t) = u_{n,k}(t)\exp(ikt)$ to the linear version of Eq. (2). Here, $u_{n,k}(t) = u_{n,k}(t + \pi)$ and k, n are the Bloch wave number and band index, respectively. Then, we obtain the linear Bloch energy spectrum through the plane-wave expansion method [44] and plot it in Fig. 1. Figures 1(b)–1(d) show the difference in the energy spectrum under different
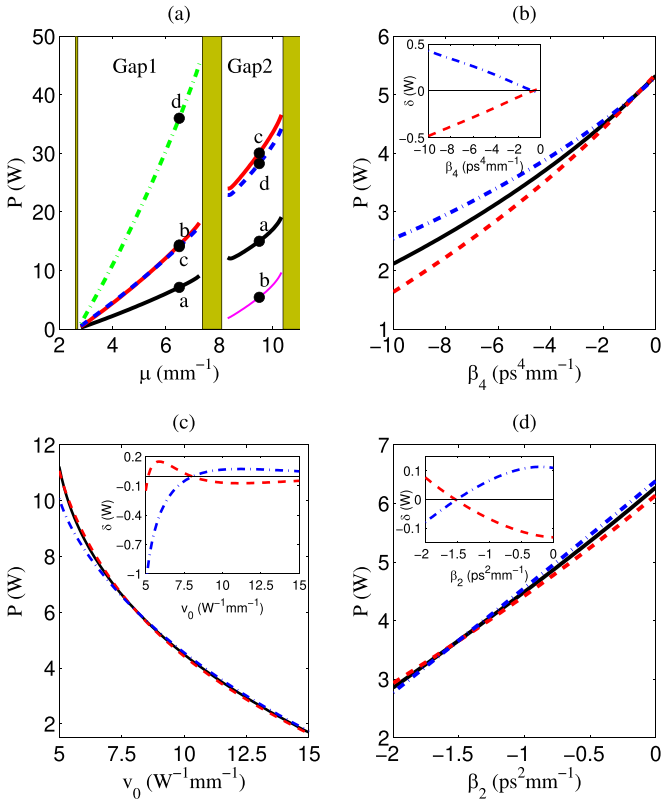
FIG. 2. Soliton power diagram. (a) $v_0 = 10$ W^{-1} mm^{-1}, $\beta_2 = -1$ ps^2 mm^{-1} and $\beta_4 = -2$ ps^4 mm^{-1}. Shadow regions are linear bands. Black (thick solid), pink (thin solid), and green (dash-dotted) lines represent FGSs, subfundamental solitons, and higher-order solitons, respectively. Red (solid near the dotted) and blue (dotted) lines are the in- and out-of-phase dipole mode, respectively. (b)–(d) Propagation constant $\mu = 4$ mm^{-1}. The solid black line represents twice the power of FGSs ($2P_0$), while the red dotted line and the blue dotted line represent the in-phase (P_{in}) and out-of-phase (P_{out}) mode, respectively. Furthermore, the invariant parameters are taken from the parameters in (a).

parameters. We particularly point out here that the parameter comparisons in this paper are all comparisons of the absolute values of the parameters. That is, when we talk about the dispersion coefficient increasing, it is actually the absolute value that increases. Therefore, when the quadratic and quartic dispersions increase, the band gap moves toward increasing propagation constant. As can be seen from Figs. 1(b) and 1(d), the width of the first gap does not noticeably change, but the second gap gradually decreases. According to Fig. 1(c), greater Bragg reflection is caused at the Brillouin zone (BZ) boundary with increased external potential intensity. The band gap gradually opens and widens from the boundary of the BZ and the bandwidth decreases, contrary to the effect of the quadratic and quartic dispersion terms. Next, we use Newton's iterative method to solve Eq. (2) on a finite difference network [45]. According to the definition of soliton power given by Eq. (3), we obtain the power diagrams of two low-order soliton families in the first and second gap; see Fig. 2(a). Among them, we study the two most typical types of higher-order solitons, i.e., in-phase and out-of-phase dipole modes [44]. The two peaks of the in-phase mode have the

same phase, as shown in Fig. 4(b), and the out-of-phase mode has the opposite phase, as shown in Fig. 4(c). In this paper, unless special emphasis is placed on the center distance of the dipole modes, the default is that the two peaks are located in two adjacent periodic potential wells. The two higher-order solitons can be regarded as a combination of FGSs. They are formed by coupling two independent FGSs under their interaction.

Since any nonlinear Schrödinger equation follows the variational principle, we introduce an energy functional of a system as an effective Hamiltonian,

$$H = \int dt \left\{ -\frac{\beta_2}{2} \left| \frac{\partial}{\partial t} \psi \right|^2 - \frac{\beta_4}{24} \left| \frac{\partial^2}{\partial t^2} \psi \right|^2 + V(t)|\psi|^2 - \frac{\gamma}{2}|\psi|^4 \right\},$$

(5)

which satisfies $i\partial\psi/\partial z = \delta H/\delta\psi^*$. When the depth of the potential well v_0 is large enough or the two solitons ϕ_1, ϕ_2 are far enough apart, the overlap of the two solitons' complex envelopes is small. In the potential well where the first soliton ϕ_1 is located, ϕ_2 tends to zero. Similarly, in the potential well where the second soliton ϕ_2 is located, ϕ_1 tends to zero. The effective Hamiltonian can be reduced to [41]

$$H = H_1 + H_2 + H_{\text{trap}} + H_{\text{int}},$$

(6)

where H_1 and H_2 are Hamiltonians of two independent FGSs. H_{trap} is the Hamiltonian caused by the interaction between the dipole modes and the external potential well, i.e., $H_{\text{trap}} = \int dt V(t)|\phi|^2$, where ϕ is the complex envelope after coupling. Due to the locality of the solitons, ϕ tends to zero in other regions outside the main potential well. Furthermore, when v_0 is sufficiently large, the external potential well can be approximately regarded as a square potential well, as shown in Fig. 6(a), i.e., the H_{trap} inside the potential well approaches zero. Under the above approximation, H_{trap} is simplified as the value at the edge of the square well, $H_{\text{trap}} = v_0|\phi(t = \text{potential well edge})|^2\delta t$, where δt is the approximate thickness of the square potential well. This value is usually greater than zero for in-phase modes and the opposite for out-of-phase modes. Moreover, its absolute value also increases as the propagation constant μ increases. For H_{int}, Refs. [40] and [41] point out that the interaction is formed by the oscillation tail of the solitons (OTS). The specific expression of H_{int} is determined by the OTS, relative phase, relative distance, propagation constant, etc. In this paper, we only consider the increase or decrease in power caused by interaction, which reflects the type of interaction between solitons. When the interaction leads to an increase in power, we call it a repulsive interaction. When it leads to a decrease in power, we call it an attractive interaction.

As seen from Figs. 3(a) and 3(b), the interaction between solitons only affects the side where the solitons are close, while the shape and OTS of the other side of the solitons remain unchanged. At the same time, the interaction between the solitons weakens as the distance between the centers of the two solitons increases, indicating that the interaction is a short-range interaction; see Figs. 3(c) and 3(d). This force plays an important role in the stability of higher-order solitons and will be discussed in detail in Sec. IV. In this section, we focus on the effect of different parameters on
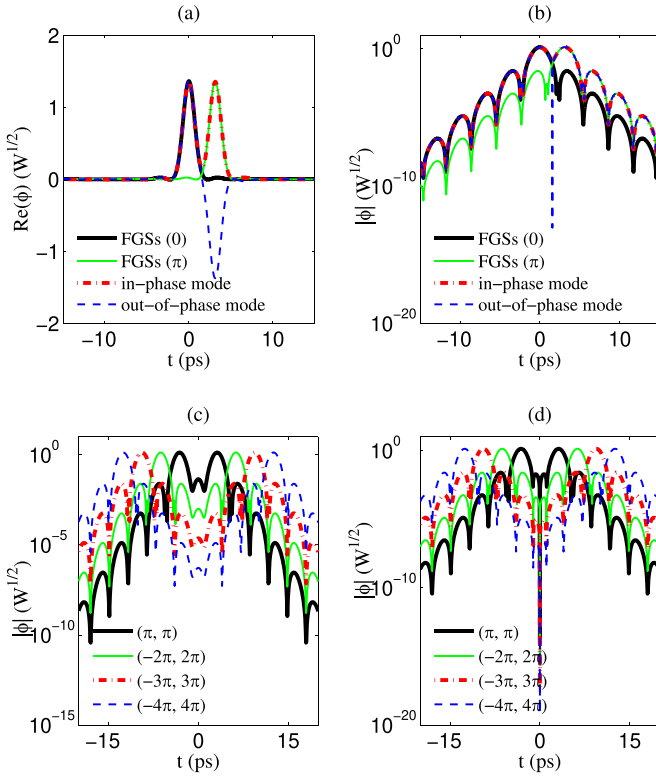
FIG. 3. Soliton profile and exponential oscillating tail for $v_0 = 10$ W^{-1} mm^{-1}, $\beta_2 = -1$ ps^2 mm^{-1}, and $\beta_4 = -2$ ps^4 mm^{-1} at $\mu = 4$ mm^{-1}. The numbers in parentheses in the figure legend indicate the center positions of FGSs and the FGSs, which compose dipole modes. For example, Figs. 4(a) and 4(b) correspond to (0) and (0, π), respectively. (c) In-phase modes. (d) Out-of-phase modes.

FIG. 4. Solitons (solid red line) and corresponding NBWs (dashed black line) at the point indicated in the first gap in Fig. 2(a) at $\mu = 6.5$ mm^{-1}. The shadow and white regions distinguish two adjacent external potential periods. The dashed blue line represents the solitons profiles, namely, the real part of the solitons, whose value corresponds to the right y axis. (a)–(d) NBWs at the center of the BZ with $N = 7.2241$, 7.2414, 6.9569, and 7.2448 W.

this interaction. To show the effects of this interaction, we define a power difference, $\delta = P_{\text{in/out}} - 2P_0$. P_{in} and P_{out} represent in- and out-of-phase mode power, respectively. P_0 represents the power of FGSs that comprise the two dipole modes. This power difference is caused by soliton-soliton and soliton–potential-well interaction.

We consider the variation in the power of independent FGSs. Since FGSs are generated in the first gap, the power is zero as they approach the bottom of the first gap. When the dispersion parameter increases, the band gap shifts upward. For a fixed propagation constant, it is equivalent to the point in the gap constantly approaching the bottom of the gap. Therefore, the soliton power decreases, which is consistent with our numerical analysis results; see solid black line in Figs. 2(b)–2(d). Then, we analyze the power differences between dipole modes and the two FGSs composed of them in different parameters. It can be found that with the increase of the quartic dispersion coefficient, the absolute value of the power difference between the two modes increases gradually, but the symbols of the two modes are different. However, quadratic dispersion produces different effects. The power difference between the two modes is gradually close to each other, and then increases in the reverse direction, but in this case, in the in-phase mode, it increases in the positive direction. The effect of v_0 is that the power difference gradually approaches zero, and the dipole is closer to the two FGSs due to suppressed tunneling, which will be mentioned later.
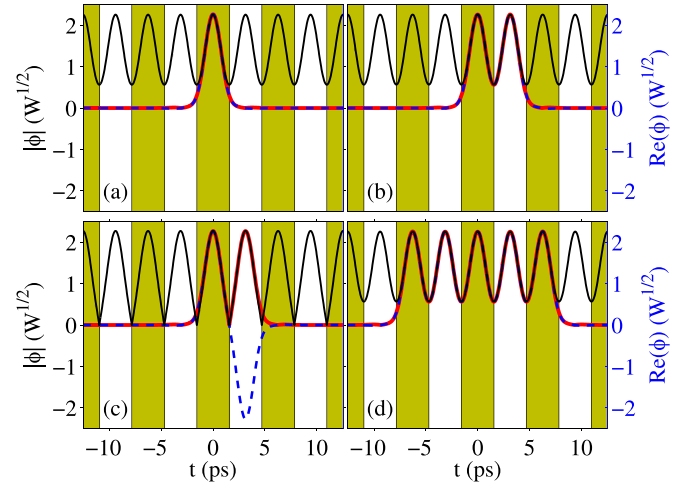
Then, we consider the relationship between solitons and NBWs. In the first gap, only one basic mode family is characterized by the peak being limited to a periodic unit, as shown in Fig. 4(a). It can be seen that it matches a periodic element of NBWs very well. In the soliton's theory, NBWs at the center or edge of the BZ are infinite chains composed of FGSs [46]. As shown in Figs. 4 and 5, the above rules apply to the system with quartic dispersion. The higher-order soliton in Fig. 4(d) comprises five FGSs by in-phase. The results show that our conclusion is correct. An alternative family of basic modes appears in the second gap, i.e., subfundamental gap solitons (sub-FGSs). Its characteristic is that it has two opposite peaks limited in a periodic unit, like the FGSs. It can be considered one of the components of the NBWs. As shown in Figs. 5(e) and 5(f), the two dipole modes are completely different from those we mentioned earlier in that they are composed of sub-FGSs, but it can still be seen that they match the NBWs quite well.

IV. STABILITY OF GAP SOLITONS

Reference [37] points out that FGSs in the first gap are stable under quadratic and quartic dispersion effects. In Fig. 7(a), we also provide stability analysis for FGSs with different parameters in the first gap, proving the correctness of this result. Due to the short-range interaction between solitons, when a sufficient distance separates the two solitons that make up the dipole, the solitons do not affect each other and are regarded as independent propagation. In this case, the stability of the dipole is consistent with that of FGSs. As the two solitons get close together, the interaction between them increases, which causes the stability of the dipole to be destroyed. According to Fig. 6(a), FGSs are confined to each period and can be regarded as a soliton trapped in the potential well, whose tail
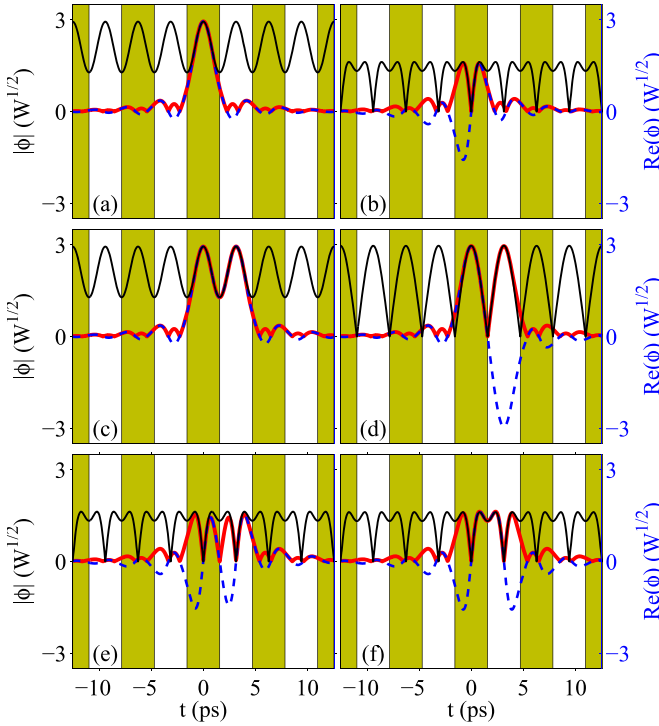
FIG. 5. Solitons (solid red line) and corresponding NBWs (dashed black line) at the point indicated in the second gap in Fig. 2(a) at $\mu = 9.5$ mm^{-1}. The shadow and white regions distinguish two adjacent external potential periods. The dashed blue line represents the solitons profiles, namely, the real part of the solitons, whose value corresponds to the right y axis. (e),(f) In-phase and out-of-phase dipole modes composed of two subfundamental solitons, respectively. (a)–(f) NBWs at the center of the BZ with $N = 15.0689$, 5.5690, 15.0862, 13.2924, 5.6034, and 5.5086 W.

FIG. 6. External potential well $V(t)$ and corresponding OTS for $v_0 = 10$ W^{-1} mm^{-1}, $\beta_2 = -1$ ps^2 mm^{-1}, $\beta_4 = -2$ ps^4 mm^{-1} at $\mu = 6.5$ mm^{-1}. (a) The solid blue and the dashed black lines represent $V(t)$ and the simplified square potential well, respectively, whose values correspond to the right y axis. Red (dashed), green (thick), and black (thin) lines, respectively, represent dipole $(0, \pi)$, dipole $(-\pi, \pi)$, with FGSs $(-\pi)$. The numbers in parentheses indicate the center position of the solitons, which are consistent with the representation of Fig. 3. (b)–(d) The shadow and white regions distinguish two adjacent external potential periods. Moreover, the solid black line represents the decaying OTS.

is represented by the tunneling of solitons. It can be seen from Figs. 6(b)–6(d) that the OTS's frequency is consistent with that of the periodic external potential well. On this basis, we analyze that when two solitons approach each other, the complex envelopes of the two solitons overlap on the side close to each other due to the action of tunneling, which is the fundamental cause of the interaction. If the interaction is repulsive, it is equivalent to enhancing the potential-well depth and weakening the tunneling effect. The two solitons tend to propagate independently. In this case, the stability of the dipole approaches that of the independent FGSs, that is, the stability increases. Conversely, when the interaction is attractive, the two solitons have a stronger coupling, which leads to a decrease in the stability of the dipole. To validate our conclusion, we will use two methods to verify the stability of stationary solutions, and look forward to the consistent results of these two methods. The first method is called linear stability analysis. Since the unstable solution is very sensitive to small disturbances, we test the stability of the solution by the disturbance complex envelope $\Psi(t, z)$,

$$
\begin{aligned}
\Psi(t, z) = [\phi(t) + u(t) \exp(i\lambda z) \\
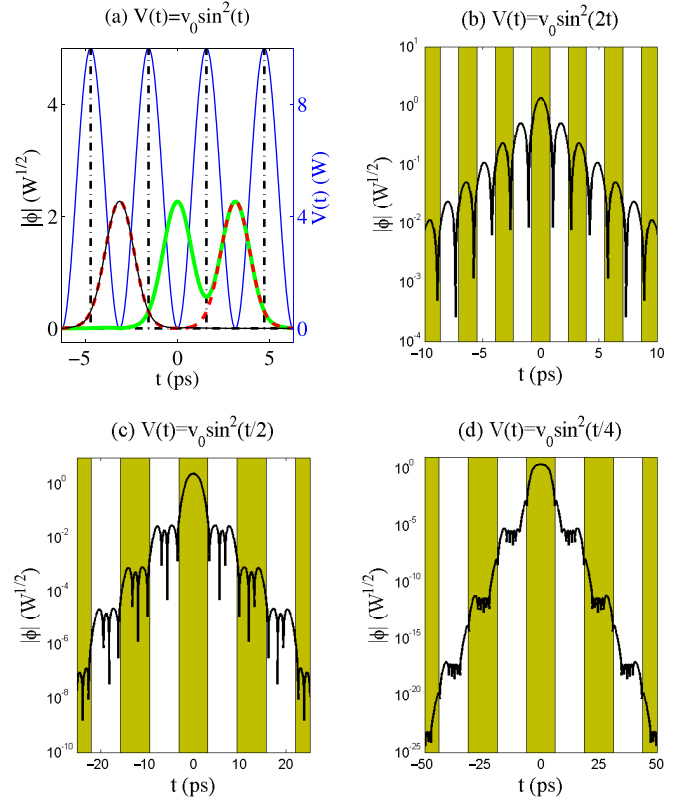+ w^*(t) \exp(-i\lambda^* z)] \exp(-i\mu z),
\end{aligned}
\tag{7}
$$

where $\phi(t)$ is the stationary solution of Eq. (2), with $u(t)$ and $w(t)$ being the small perturbations at eigenvalue λ. By substituting the perturbation solution $\Psi(t, z)$ to Eq. (2), the following eigenvalue problem can be obtained:

$$
\begin{pmatrix} L & \gamma\phi^2 \\ -\gamma\phi^{*2} & -L \end{pmatrix} \begin{pmatrix} u \\ w \end{pmatrix} = \lambda \begin{pmatrix} u \\ w \end{pmatrix},
\tag{8}
$$

with $L = -\frac{\beta_2}{2}\frac{d^2}{dt^2} + \frac{\beta_4}{24}\frac{d^4}{dt^4} - v_0 \sin^2(t) + 2\gamma|\phi|^2 + \mu$. In Eq. (8), when the imaginary part of the eigenvalue λ is zero, we call the stationary solution $\phi(t)$ robust stability. When it is nonzero, it is unstable.

Figures 7(c)–7(e) show that for in-phase modes, there is a sudden and abnormal drop in soliton power difference near the top of the band gap. This is because as the propagation constant increases, the OTS strength increases, leading to a stronger coupling between FGSs; see Fig. 7(b). From the perspective of physics, this can be interpreted as soliton energy increasing, but the depth of the potential well is changeless, and tunneling increases as a result. Moreover, the complex envelopes are superimposed because the in-phase modes are
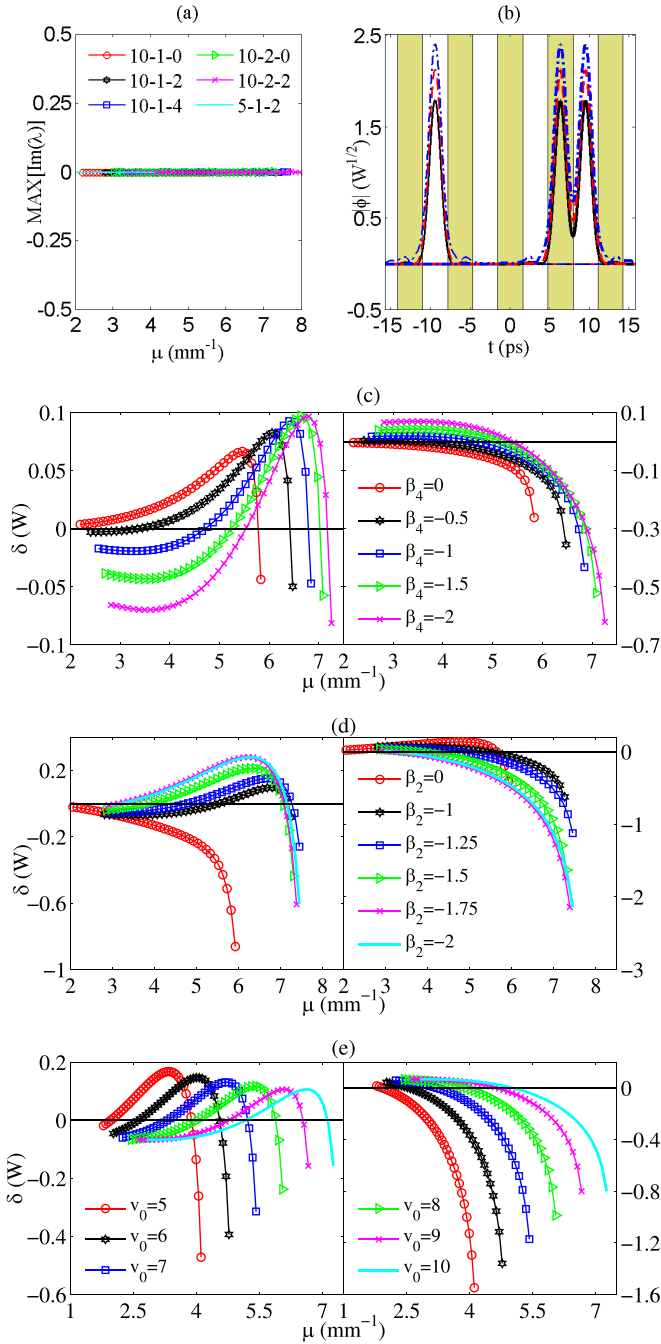
FIG. 7. Linear stability analysis of FGSs and dipole modes' power difference in the first gap. (a) The numbers in the figure legend are the values of v_0, $-\beta_2$, and $-\beta_4$, separated by hyphens. For example, "$10-1-1$" indicates $v_0 = 10$ W^{-1} mm^{-1}, $\beta_2 = -1$ ps^2 mm^{-1}, and $\beta_4 = -1$ ps^4 mm^{-1}. (b) Black (solid), red (dashed), and blue (dash-dotted) lines represent $\mu = 5, 6$, and 7 mm^{-1}, respectively. The thin lines are FGSs, and the thick lines are the in-phase mode. (c)–(e) The left panels represent in-phase modes and the right panels represent out-of-phase modes. The invariant parameters are taken from $v_0 = 10$ W^{-1} mm^{-1}, $\beta_2 = -1$ ps^2 mm^{-1}, and $\beta_4 = -2$ ps^4 mm^{-1}. The content is in one-to-one correspondence with Fig. 8.

composed of two FGSs in phase. So, the coupling part cannot simply be regarded as the disturbance part, Eq. (6) is no longer applicable, and the definition of δ is also no longer satisfied.
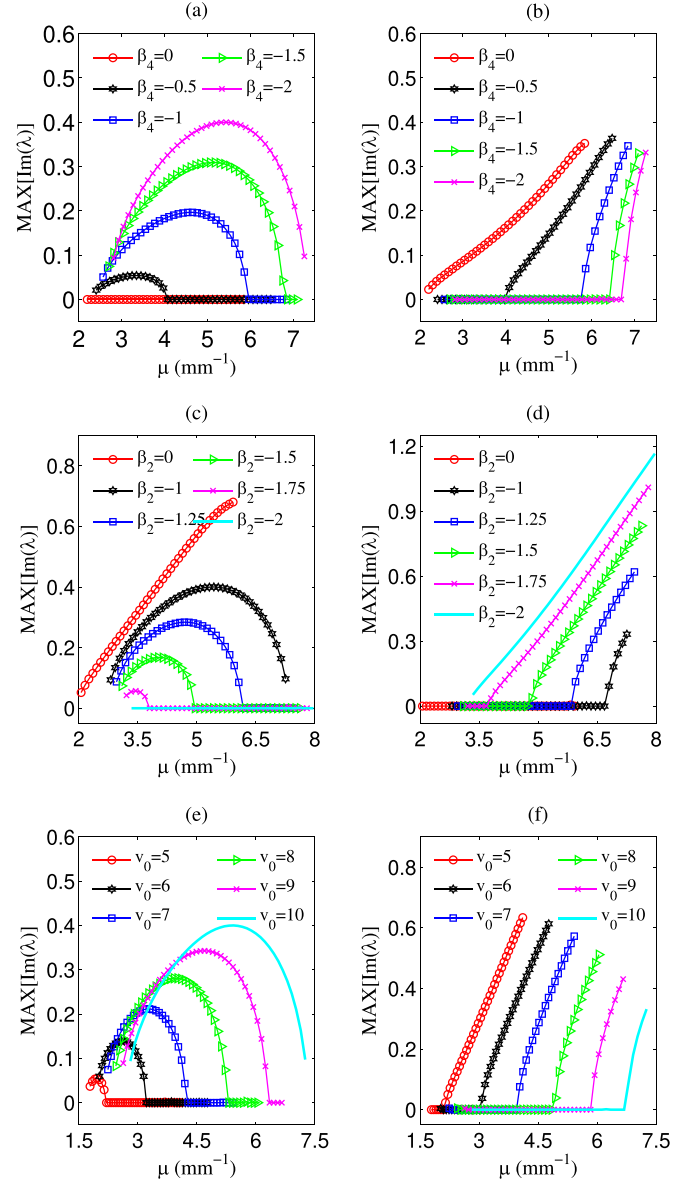

FIG. 8. Linear stability analysis. The maximum imaginary part of the eigenvalue varies with μ under different parameters in the first gap. (a),(c),(e) The stabilities of the in-phase mode; (b),(d),(f) the out-of-phase mode. Their unchanged parameters are taken from $v_0 = 10$ W^{-1} mm^{-1}, $\beta_2 = -1$ ps^2 mm^{-1} and $\beta_4 = -2$ ps^4 mm^{-1}.

Since δ is composed of two parts, we should remove the soliton–potential-well interaction part, $\delta_{int} = \delta - \delta_{well}$. For in-phase solitons, it is equivalent to moving δ in the decreasing direction, while out-of-phase is moving in the increasing direction, but these do not change the trend of δ. So we can still distinguish the change of stability by the change of δ. Since the FGSs' power tends to zero at the bottom of the first gap and the power variation δ_{well} caused by the external potential well also tends to zero, we use this as the basis for stability judgment. When the part near the top of the band gap is not considered, it can be seen from Fig. 7(c) that when $\beta_4 = 0$ ps^4 mm^{-1}, the in-phase mode power difference δ is always greater than zero, which indicates the repulsive interaction and enhanced stability. From this conclusion, we
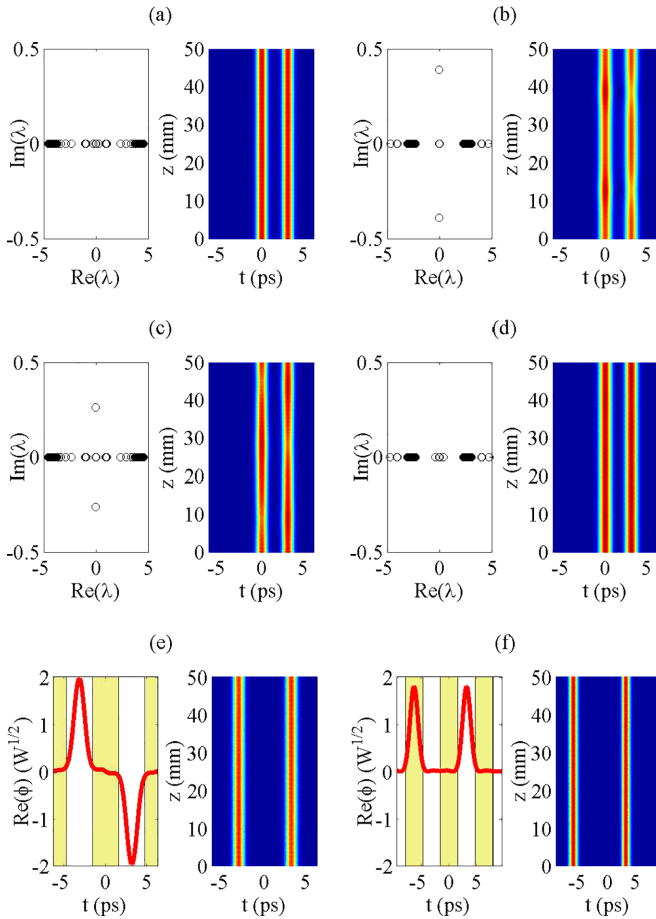
FIG. 9. Linear stability analysis and real-time evolution with 10% noise added at $\mu = 5$ mm^{-1}. Parameters corresponding to the three figures on the left are $v_0 = 10$ W^{-1} mm^{-1}, $\beta_2 = -1$ ps^2 mm^{-1}, and $\beta_4 = 0$ ps^4 mm^{-1}, and the right has a different parameter, which is $\beta_4 = -2$ ps^4 mm^{-1}. In the evolution diagram on the right panel, the color represents $|\phi(t)|^2$. (a),(b) In-phase mode. (c),(d) Out-of-phase mode. (e) Out-of-phase mode $(-\pi, \pi)$ in which the central position differs by two periods. (f) In-phase mode $(-2\pi, \pi)$. The shadow and white regions distinguish two adjacent external potential periods in the left panel of (e) and (f).

can conclude that in the first gap, when $\beta_4 = 0$ ps^4 mm^{-1}, the in-phase mode is stable throughout the first gap, while the out-of-phase mode is the opposite because its power difference is always less than zero. In addition, as can be seen from Fig. 7(c), with the increase of β_4, the in-phase mode is unstable at the bottom of the band gap and the unstable region keeps expanding. However, after a certain point, the instability decreases because the interaction changes from attractive to repulsive as μ increases. The out-of-phase mode is stable at the bottom of the band gap, and the stability region becomes larger when β_4 increases. Nonetheless, the stability decreases after a point, indicating that the out-of-phase mode is unstable in the large propagation constant region. These results are consistent with the numerical analysis results of Figs. 8(a) and 8(b). Other cases are consistent with the above analysis and can be seen to be consistent with the linear stability analysis results. Furthermore, Figs. 7(c)–7(e) show that the power difference can show stability under different parameters at the
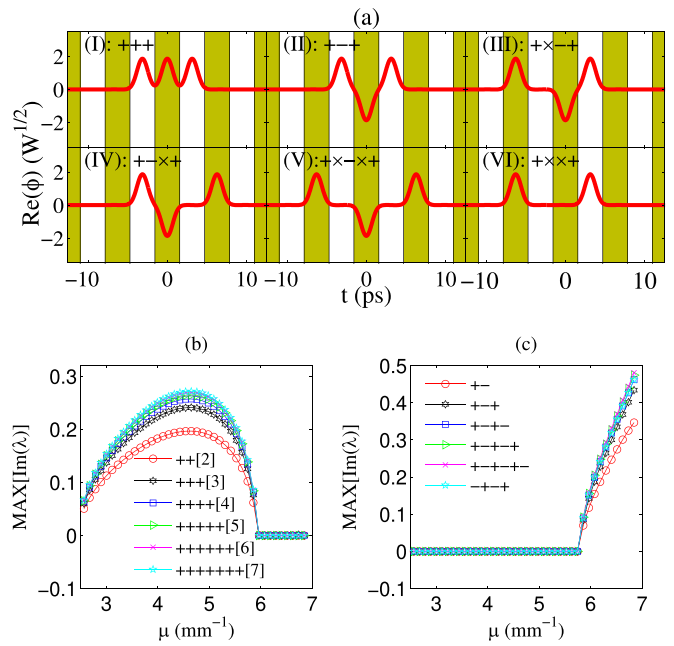

FIG. 10. Type of gap waves and linear stability analysis for $v_0 = 10$ W^{-1} mm^{-1}, $\beta_2 = -1$ ps^2 mm^{-1}, and $\beta_4 = -1$ ps^4 mm^{-1}. The shadow and white regions distinguish two adjacent external potential periods.

fixed propagation constant. The smaller δ is, the less stable it is. We use the maximum value of the imaginary part λ to represent the degree of instability. When the dipole modes are unstable, a smaller δ will cause a larger [MAXIm(λ)] in the linear stability analysis. We use the second method to verify the results of linear stability analysis. We add 10% Gaussian noise to the stationary solution to simulate the disturbance, take results after a disturbance as the initial condition of Eq. (1), and use the second-order time-splitting step method [47] and Crank-Nicolson method [48] to monitor its evolution; see the Appendix for details. If it grows or decays with the development of the system, we call it unstable. Otherwise, it is robust stable. This method is called real-time evolution. As shown in Fig. 9, we show some real-time evolution results, which are consistent with our linear stability analysis results. It can be seen that with the evolution of the system, in the stable area, the unstable state caused by disturbance will decay rapidly and transform into a stable soliton shape, and then the soliton morphology will remain unchanged. However, solitons in the unstable region will fluctuate and even diverge in evolution. Since the interaction between solitons is a short-range interaction, when the dipole is unstable, we can increase the central distance between the two FGSs to reduce the interaction between solitons, thus increasing the stability of the composed dipole. The real-time evolution results are shown in Figs. 9(b), 9(e), 9(c), and 9(f).

V. GAP WAVES

This section focuses on higher-order solitons, often called gap waves. Among them, the dipoles mentioned in Sec. IV are special gap waves composed of two FGSs. We use the previous conclusions to directly obtain the stability of some gap waves without numerical analysis. To better illustrate our
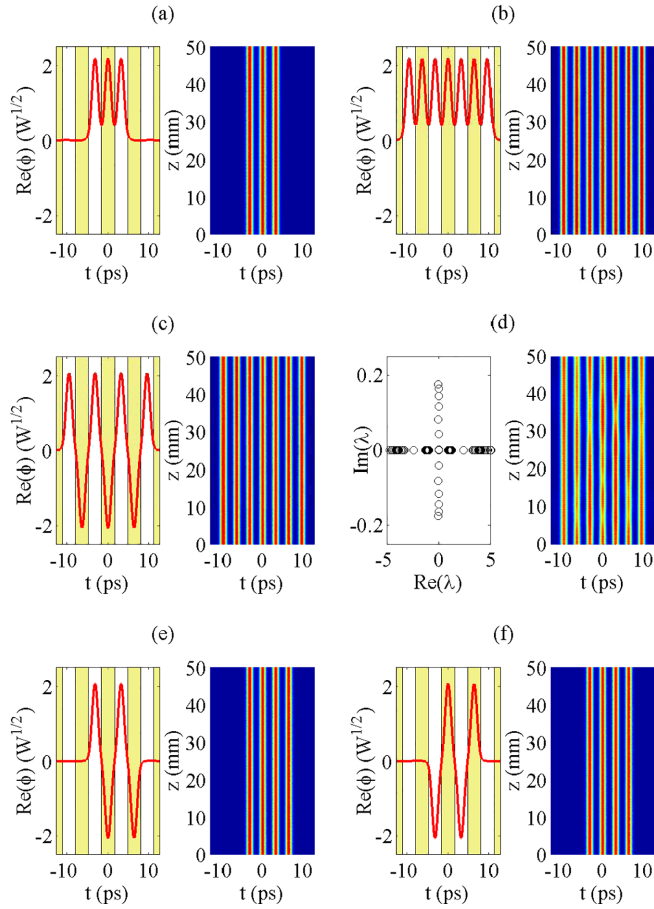
FIG. 11. Soliton profile and real-time evolution with 10% noise for $v_0 = 10$ W^{-1} mm^{-1}, $\beta_2 = -1$ ps^2 mm^{-1}, and $\beta_4 = -1$ ps^4 mm^{-1}. In the soliton profile figure, the shadow and white regions distinguish two adjacent external potential periods. In the evolution diagram on the right panel, the color represents $|\phi(t)|^2$. (a) "$+++$" mode at $\mu = 6$ mm^{-1}. (b) "$++++++$" mode at $\mu = 6$ mm^{-1}. (c),(d) "$+-+-+-+$" mode at $\mu = 5.6$ and 6 mm^{-1}, respectively. (e),(f) "$+-+-$" and "$-+-+$" modes at $\mu = 5.6$ mm^{-1}, respectively.

conclusions, we explain the symbols that appear later. We define the peak of the soliton profile in the positive half-axis part as a "$+$" mode and a "$-$" mode in the negative half-axis part. We use the "$\times$" mode to represent the part without a peak between the two peaks. The more "$\times$" between the two peaks, the farther apart the soliton centers are. Due to the localization of solitons, each peak of the gap waves formed by FGSs is confined to a unit cell, so each symbol represents a unit cell and is described from the first crest encountered in the negative direction. In Fig. 10(a), we give some gap waves and name them using our definition. Since the short-range interaction between solitons affects only the close side, we do not destroy the stability when we add FGSs successively in the same relative phase based on the dipole models. For example, if "$++$" continues to add "$+$" mode, that is, to add FGSs in the same phase, then the gap waves under this construction should get the same stable interval. We used linear stability analysis and real-time evolution to obtain consistent results, as shown in Figs. 10(b), 11(a), and 11(b). The out-of-phase
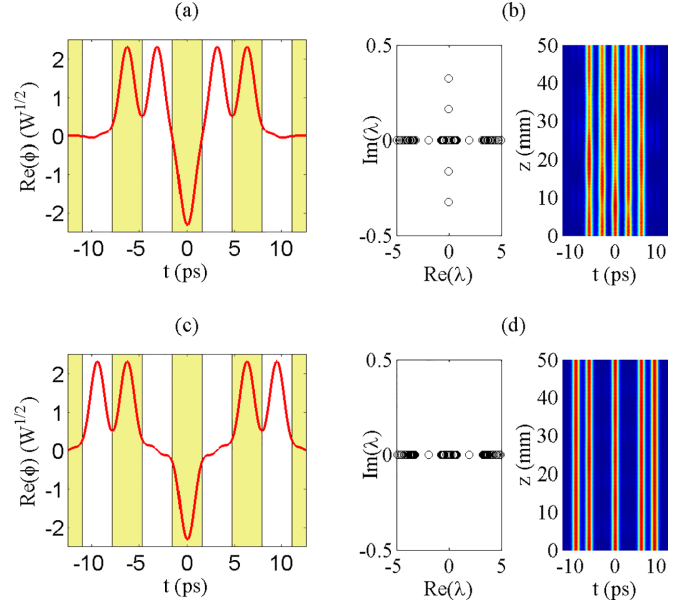

FIG. 12. Soliton profile, linear stability analysis, and real-time evolution with 10% noise added for $v_0 = 10$ W^{-1} mm^{-1}, $\beta_2 = -1$ ps^2 mm^{-1}, and $\beta_4 = -1$ ps^4 mm^{-1} at $\mu = 6.5$ mm^{-1}. (a),(b) "$++-++$" mode. (c),(d) "$++\times-\times++$" mode. In the evolution diagram, the color represents $|\phi(t)|^2$.

mode "$+-$" is obtained by successively adding FGSs in reverse phase to obtain gap waves such as "$+-+$," "$+-+-$," and "$-+-+$," which should also maintain the same stable interval, as shown in Figs. 10(c), 11(c), and 11(d). If the way of constructing gap waves is reversed, that is, the "$+-+-$" mode is changed into the "$-+-+$" mode, it can be easily known from Eq. (8) that the stability will not change at all. Figures. 11(e) and 11(f) verify this conclusion. In fact, there is no difference between the "$+-$" and "$-+$" modes. We can only see that this is a gap wave composed of two FGSs by out-of-phase combination, so its stability will not change, which also verifies the correctness of our linear stability analysis and real-time evolution. In the process of constructing gap waves, a phase different from the law will lead to a huge change in the stability of the gap waves, for instance, the "$+++++$" and "$++-++$" modes. From the linear stability analysis results of Fig. 10(b), it can be seen that the "$+++++$" mode is stable at $\mu = 6.5$ mm^{-1}, but Fig. 12(b) shows that the "$++-++$" mode is unstable. In that case, we can still increase the distance between the abnormal mode and the center of the surrounding FGSs to restore stability, like the "$++\times-\times++$" mode; see Fig. 12(d).

VI. CONCLUSION

In conclusion, through numerical calculation, we find the gap solitons produced by the competition between the quadratic dispersion, quartic dispersion, and Kerr nonlinearity. Compared with the NBWs, FGSs can still be regarded as a basic component of the NBWs. We then investigate the effect of parameter variations on the power of the two classical dipole modes. The results show that the quadratic and quartic dispersion have opposite effects on the power caused

by changes in the interaction between the two FGSs that make up the dipole mode. We analyze this interaction and find a short-range action generated by the decaying OTS. The action only affects the side of the two solitons close to each other, and the OTS's frequency is the same as that of the external potential well. We define different interaction types by comparing the power difference between the dipole model and FGSs. Furthermore, we analyze the effect of this interaction on the stability of the dipole model, with results consistent with linear stability analysis and real-time evolution. Finally, we adopt the interaction analysis to directly present the stability of gap waves, consistent with the results obtained from the numerical analysis. In addition, some possible methods are given to stabilize some unstable gap waves, which provides a method to regulate the stability of higher-order solitons.

APPENDIX: NUMERICAL METHODS

In this Appendix, we briefly introduce numerical schemes for simulating soliton evolution. The method combines the second-order time-splitting step method and the Crank-Nicolson method. First, we divide the nonlinear Schrödinger equation (1) into a linear part and a nonlinear part as follows:

$$i\frac{\partial \psi}{\partial z} = (H_{\text{lin}} + H_{\text{non}})\psi, \tag{A1}$$

with

$$H_{\text{lin}} = \frac{\beta_2}{2}\Delta_t - \frac{\beta_4}{24}\Delta_t^2 + V(t), \quad H_{\text{non}} = -\gamma|\psi|^2. \tag{A2}$$

Here, Δ_t is the Laplace operator expressed as $\partial^2/\partial t^2$. For a better description, we introduce some notation here. Let m and p be two positive integers. The interval $[-T,\ T]$ is equally divided into m parts, and the step size in the t direction is $h_t = 2T/m$. The interval $[0,\ Z]$ is divided into p parts, and the step size in the z direction is $h_z = Z/p$. Let us call $t_j = jh_t(-m/2 \leqslant j \leqslant m/2)$, $z_n = nh_z(0 \leqslant n \leqslant p)$. Now we introduce the following notation: ψ_j^n is the value of the complex envelope at $(t_j = jh_z, z_n = nh_z)$; ψ^n represents all values of the complex envelope in the t direction at $z_n = nh_z$, which is an $m \times 1$ column vector.

According to the idea of the "time"-splitting step method, we decompose Eq. (A1) at each z level and then calculate it step by step to obtain the following form:

$$\psi^{n+1} = e^{-iH_{\text{non}}h_z/2}e^{-iH_{\text{lin}}h_z}e^{-iH_{\text{non}}h_z/2}\psi^n. \tag{A3}$$

This method is also known as Strang splitting. In order to improve the accuracy of the simulation, we use the Crank-Nicolson method for the calculation of the linear part, which is of the form

$$\frac{\psi_j^{n+1} - \psi_j^n}{h_z} = \frac{1}{2}F_j^{n+1}\big(t, z, \Delta_t, \Delta_t^2\big) + \frac{1}{2}F_j^n\big(t, z, \Delta_t, \Delta_t^2\big). \tag{A4}$$

By substituting Eq. (A4) into the linear version of Eq. (1), we get

$$(I + A - B - C)\psi^{n+1} = (I - A + B + C)\psi^n, \tag{A5}$$

where

$$A = \frac{1}{2}\text{coeff}_1 \begin{pmatrix} -2 & 1 & & & & \\ 1 & -2 & 1 & & & \\ & \ddots & \ddots & \ddots & & \\ & & 1 & -2 & 1 \\ & & & 1 & -2 \end{pmatrix}, \tag{A6}$$

$$B = \frac{1}{2}\text{coeff}_2 \begin{pmatrix} 5 & -4 & 1 & & & & \\ -4 & 6 & -4 & 1 & & & \\ 1 & -4 & 6 & -4 & 1 & & \\ & \ddots & \ddots & \ddots & \ddots & \ddots & \\ & & 1 & -4 & 6 & -4 & 1 \\ & & & 1 & -4 & 6 & -4 \\ & & & & 1 & -4 & 5 \end{pmatrix}, \tag{A7}$$

with

$$\text{coeff}_1 = -\frac{\beta_2 h_z}{2ih_t^2}, \quad \text{coeff}_2 = -\frac{\beta_4 h_z}{24ih_t^4}, \tag{A8}$$

and I is the identity matrix, and C is the diagonalized matrix of $V(t)$. The vertical bars in the matrix are used only to distinguish between two adjacent columns and have no practical meaning. We define $M = (I + A - B - C)^{-1}(I - A + B + C)$ and give a numerical scheme within a loop,

$$\psi^{n+\frac{1}{2}} = \exp(i\gamma|\psi^n|^2 h_z/2)\psi^n,$$
$$\tilde{\psi}^{n+\frac{1}{2}} = M\psi^{n+\frac{1}{2}},$$
$$\psi^{n+1} = \exp\big(i\gamma|\tilde{\psi}^{n+\frac{1}{2}}|^2 h_z/2\big)\tilde{\psi}^{n+\frac{1}{2}n}. \tag{A9}$$

In the above process, the product between column vectors and column vectors is expressed as the corresponding element multiplication, i.e., Hadamard product. At the beginning of the simulation, we denote the perturbed complex envelope as ψ^0; then, by repeating the Eq. (A9) process, we can simulate solitons of any z value.

[1] C. S. Gardner, J. M. Greene, M. D. Kruskal, and R. M. Miura, Method for Solving the Korteweg-deVries Equation, Phys. Rev. Lett. **19**, 1095 (1967).

[2] N. J. Zabusky and M. D. Kruskal, Interaction of "Solitons" in a Collisionless Plasma and the Recurrence of Initial States, Phys. Rev. Lett. **15**, 240 (1965).

[3] V. M. Pérez-García, H. Michinel, and H. Herrero, Bose-Einstein solitons in highly asymmetric traps, Phys. Rev. A **57**, 3837 (1998).

[4] R. Carretero-González, D. J. Frantzeskakis, and P. G. Kevrekidis, Nonlinear waves in Bose–Einstein condensates: Physical relevance and mathematical techniques, Nonlinearity **21**, R139 (2008).

[5] J. N. Elgin, Perturbations of optical solitons, Phys. Rev. A **47**, 4331 (1993).

[6] E. B. Kolomeisky and E. Sarabamoun, Solitons in the Einstein universe, Phys. Rev. D **101**, 043515 (2020).

[7] M. A. Porras, Spatiotemporal optical vortex solitons: Dark solitons with transverse and tilted phase line singularities, Phys. Rev. A **104**, L061502 (2021).

[8] J. T. Cole, K. G. Makris, Z. H. Musslimani, D. N. Christodoulides, and S. Rotter, Twofold $\mathcal{PT}$ symmetry in doubly exponential optical lattices, Phys. Rev. A **93**, 013803 (2016).

[9] Y. V. Kartashov, V. V. Konotop, and F. K. Abdullaev, Gap Solitons in a Spin-Orbit-Coupled Bose-Einstein Condensate, Phys. Rev. Lett. **111**, 060402 (2013).

[10] T. F. Xu, X. M. Guo, X. L. Jing, W. C. Wu, and C. S. Liu, Gap solitons and Bloch waves of interacting bosons in one-dimensional optical lattices: From the weak- to the strong-interaction limits, Phys. Rev. A **83**, 043610 (2011).

[11] S. L. Palacios, Optical solitons in highly dispersive media with a dual-power nonlinearity law, J. Opt. A: Pure Appl. Opt. **5**, 180 (2003).

[12] S. L. Palacios and J. M. Fernández-Díaz, Black optical solitons for media with parabolic nonlinearity law in the presence of fourth order dispersion, Opt. Commun. **178**, 457 (2000).

[13] A. Blanco-Redondo, C. M. de Sterke, J. E. Sipe, T. F. Krauss, B. J. Eggleton, and C. Husko, Pure-quartic solitons, Nat. Commun. **7**, 10427 (2016).

[14] A. F. J. Runge, D. D. Hudson, K. K. K. Tam, C. M. de Sterke, and A. Blanco-Redondo, The pure-quartic soliton laser, Nat. Photon. **14**, 492 (2020).

[15] Y. Yıldırım, A. Biswas, M. Asma, P. Guggilla, S. Khan, M. Ekici, A. K. Alzahrani, and M. R. Belic, Pure-cubic optical soliton perturbation with full nonlinearity, Optik **222**, 165394 (2020).

[16] J. Widjaja, E. Kobakhidze, T. R. Cartwright, J. P. Lourdesamy, A. F. J. Runge, T. J. Alexander, and C. M. de Sterke, Absence of Galilean invariance for pure-quartic solitons, Phys. Rev. A **104**, 043526 (2021).

[17] J. Zeng, J. Dai, W. Hu, and D. Lu, Theory for the interaction of pure-quartic solitons, Appl. Math. Lett. **129**, 107923 (2022).

[18] A. F. J. Runge, T. J. Alexander, J. Newton, P. A. Alavandi, D. D. Hudson, A. Blanco-Redondo, and C. M. de Sterke, Self-similar propagation of optical pulses in fibers with positive quartic dispersion, Opt. Lett. **45**, 3365 (2020).

[19] K. K. K. Tam, T. J. Alexander, A. Blanco-Redondo, and C. M. de Sterke, Generalized dispersion Kerr solitons, Phys. Rev. A **101**, 043822 (2020).

[20] W.-J. Liu, B. Tian, H.-Q. Zhang, T. Xu, and H. Li, Solitary wave pulses in optical fibers with normal dispersion and higher-order effects, Phys. Rev. A **79**, 063810 (2009).

[21] A. Choudhuri and K. Porsezian, Impact of dispersion and non-Kerr nonlinearity on the modulational instability of the higher-order nonlinear Schrödinger equation, Phys. Rev. A **85**, 033820 (2012).

[22] C. Milián, A. V. Gorbach, M. Taki, A. V. Yulin, and D. V. Skryabin, Solitons and frequency combs in silica microring resonators: Interplay of the Raman and higher-order dispersion effects, Phys. Rev. A **92**, 033851 (2015).

[23] E. N. Tsoy and C. M. de Sterke, Theoretical analysis of the self-frequency shift near zero-dispersion points: Soliton spectral tunneling, Phys. Rev. A **76**, 043804 (2007).

[24] V. I. Kruglov and H. Triki, Quartic and dipole solitons in a highly dispersive optical waveguide with self-steepening nonlinearity and varying parameters, Phys. Rev. A **102**, 043509 (2020).

[25] H. Triki and V. I. Kruglov, Propagation of dipole solitons in inhomogeneous highly dispersive optical-fiber media, Phys. Rev. E **101**, 042220 (2020).

[26] V. I. Kruglov and J. D. Harvey, Solitary waves in optical fibers governed by higher-order dispersion, Phys. Rev. A **98**, 063811 (2018).

[27] K. Nithyanandan, R. V. J. Raja, K. Porsezian, and B. Kalithasan, Modulational instability with higher-order dispersion and walk-off in Kerr media with cross-phase modulation, Phys. Rev. A **86**, 023827 (2012).

[28] Y. L. Qiang, T. J. Alexander, and C. M. de Sterke, Generalized sixth-order dispersion solitons, Phys. Rev. A **105**, 023501 (2022).

[29] A. F. J. Runge, T. J. Alexander, H. P. Talathi, D. D. Hudson, A. Blanco-Redondo, and C. M. de Sterke, Generalized self-similar propagation and amplification of optical pulses in nonlinear media with high-order normal dispersion, Phys. Rev. A **104**, 013506 (2021).

[30] A. F. J. Runge, Y. L. Qiang, T. J. Alexander, M. Z. Rafat, D. D. Hudson, A. Blanco-Redondo, and C. M. de Sterke, Infinite hierarchy of solitons: Interaction of Kerr nonlinearity with even orders of dispersion, Phys. Rev. Res. **3**, 013166 (2021).

[31] K. K. Ndebele, C. B. Tabi, Camus G. Latchio Tiofack, and T. C. Kofané, Higher-order dispersion and nonlinear effects of optical fibers under septic self-steepening and self-frequency shift, Phys. Rev. E **104**, 044208 (2021).

[32] L. Ge, M. Shen, C. Ma, T. Zang, and L. Dai, Gap solitons in PT-symmetric optical lattices with higher-order diffraction, Opt. Express **22**, 29435 (2014).

[33] C. G. L. Tiofack, F. I. Ndzana, A. Mohamadou, and T. C. Kofane, Spatial solitons and stability in the one-dimensional and the two-dimensional generalized nonlinear Schrödinger equation with fourth-order diffraction and parity-time-symmetric potentials, Phys. Rev. E **97**, 032204 (2018).

[34] R. Parker and A. Aceves, Multi-pulse solitary waves in a fourth-order nonlinear Schrödinger equation, Physica D **422**, 132890 (2021).

[35] J. Li, Y. Zhang, and J. Zeng, Dark gap solitons in one-dimensional nonlinear periodic media with fourth-order dispersion, Chaos Solitons Fractals **157**, 111950 (2022).

[36] R. I. Bandara, A. Giraldo, N. G. R. Broderick, and B. Krauskopf, Infinitely many multipulse solitons of different symmetry types in the nonlinear Schrödinger equation with quartic dispersion, Phys. Rev. A **103**, 063514 (2021).

[37] J. T. Cole and Z. H. Musslimani, Band gaps and lattice solitons for the higher-order nonlinear Schrödinger equation with a periodic potential, Phys. Rev. A **90**, 013815 (2014).

[38] D. E. Pelinovsky, A. A. Sukhorukov, and Y. S. Kivshar, Bifurcations and stability of gap solitons in periodic potentials, Phys. Rev. E **70**, 036618 (2004).

[39] A. Stefanov, G. A. Tsolias, J. Cuevas-Maraver, and P. G. Kevrekidis, Mixed dispersion nonlinear Schrödinger

equation in higher dimensions: Theoretical analysis and numerical computations, J. Phys. A: Math. Theor. **55**, 265701 (2022).

[40] N. N. Akhmediev and A. V. Buryak, Interactions of solitons with oscillating tails, Opt. Commun. **121**, 109 (1995).

[41] A. V. Buryak and N. N. Akhmediev, Stability criterion for stationary bound states of solitons with radiationless oscillating tails, Phys. Rev. E **51**, 3572 (1995).

[42] T. J. Alexander, G. A. Tsolias, A. Demirkaya, R. J. Decker, C. M. de Sterke, and P. G. Kevrekidis, Dark solitons under higher-order dispersion, Opt. Lett. **47**, 1174 (2022).

[43] G. Hwang, T. R. Akylas, and J. Yang, Gap solitons and their linear stability in one-dimensional periodic media, Physica D **240**, 1055 (2011).

[44] Y. Zhang, Y. Xu, and T. Busch, Gap solitons in spin-orbit-coupled Bose-Einstein condensates in optical lattices, Phys. Rev. A **91**, 043629 (2015).

[45] S. Wu, C. Huang, and Y. Liu, Newton waveform relaxation method for solving algebraic nonlinear equations, Appl. Math. Comput. **201**, 553 (2008).

[46] Y. Zhang, Z. Liang, and B. Wu, Gap solitons and Bloch waves in nonlinear periodic systems, Phys. Rev. A **80**, 063815 (2009).

[47] S. Yu, S. Zhao, and G. Wei, Local spectral time splitting method for first- and second-order partial differential equations, J. Comput. Phys. **206**, 727 (2005).

[48] J. Yang and T. I. Lakoba, Universally-convergent squared-operator iteration methods for solitary waves in general nonlinear wave equations, Stud. Appl. Math. **118**, 153 (2007).